Electron plasma wake field acceleration in solar coronal and chromospheric plasmas

David Tsiklauri

Citation: Physics of Plasmas **24**, 072902 (2017); doi: 10.1063/1.4990560
View online: http://dx.doi.org/10.1063/1.4990560
View Table of Contents: http://aip.scitation.org/toc/php/24/7
Published by the American Institute of Physics

Electron plasma wake field acceleration in solar coronal and chromospheric plasmas

David Tsiklauri
School of Physics and Astronomy, Queen Mary University of London, London E1 4NS, United Kingdom

(Received 19 May 2017; accepted 14 June 2017; published online 29 June 2017)

Three dimensional, particle-in-cell, fully electromagnetic simulations of electron plasma wake field acceleration applicable to the solar atmosphere are presented. It is established that injecting driving and trailing electron bunches into solar coronal and chromospheric plasmas results in electric fields $(-(20-5)\times 10^6$ V/m), leading to acceleration of the trailing bunch up to 52 MeV, starting from initial 36 MeV. The results provide one of the potentially important mechanisms for the extremely energetic solar flare electrons, invoking plasma wake field acceleration. *Published by AIP Publishing*. [http://dx.doi.org/10.1063/1.4990560]

I. INTRODUCTION

Large solar flares can accelerate particles which travel into interplanetary space and also smash into the Sun producing X-rays and gamma-rays and cause Earth ionospheric response. Detailed theoretical models exist, which consider various aspects of the generation of x-rays in solar flares.[1] Occasionally, ions are accelerated to few GeV and electrons to in excess of 100 MeV.[2] There are also some extremely energetic solar flare events, the so-called electron-dominated flares, see, e.g., Sec. 14.2.1 from Aschwanden,[3] where upper energy cutoff provides a true lower limit of the maximum energy of accelerated electrons. In some cases, the maximum electron energy can be as high as 50 MeV or more. Such high energies pose a problem for conventional electron acceleration mechanisms:[4] routinely measuring (for the 185 flare events) electrons with 10–25 MeV energies in excess of the composite photon spectral model. Moses *et al.*[5] present 55 event surveys of energy spectra of 0.1–100 MeV interplanetary electrons originating from solar flares as measured by two spectrometers on board the ISEE 3 (ICE) spacecraft. In this work, we apply a novel mechanism, the electron plasma wake field acceleration (PWFA), to solar coronal and chromospheric plasma extremely energetic solar flare events.

The basic concepts of plasma acceleration based on laser wake field acceleration (LWFA) were originally conceived by Tajima and Dawson.[6] Initial experiments for the plasma wake field were implemented by Joshi.[7] Usually, a distinction is made what creates the plasma wake: a laser or a charged particle beam. The latter case is referred to as plasma wake field acceleration (PWFA), while the former is referred to as laser wake field acceleration (LWFA). Current experimental devices show accelerating gradients several orders of magnitude better (10 s of GeV m^{-1}) than current RF-based conventional particle accelerators (10 s of MeV m^{-1}). Litos *et al.*[8] made a significant progress in PWFA. In their plasma wake field accelerator, the plasma wave is created by a 20-GeV electron bunch from SLAC's linac. A second bunch of equally energetic electrons follows close behind. With SLAC's purpose-built Facility for Advanced Accelerator Experimental Tests (FACET),[9] authors could place the trailing bunch at just the right spot in the plasma wave to increase the bunch energy by 1.6 GeV over just 30 cm of plasma.

Also there has been interesting progress in applying PWFA concepts to astrophysical plasmas. This includes astrophysical ZeV acceleration in the relativistic jet from an accreting supermassive blackhole,[10,11] focusing on ponderomotive acceleration by relativistic waves[12] and electromagnetic aspects.[13] A comprehensive, recent review is available.[14]

In a recent work of Pechhacker and Tsiklauri,[15] a beam of accelerated electrons was injected into a magnetized, Maxwellian, homogeneous, and inhomogeneous background plasma. It was established that in the case of increasing density along the path of an electron beam wave-particle resonant interaction of Langmuir waves (the same type of wave as in plasma wake field acceleration) with the beam electrons leads to an efficient particle acceleration. This is due to the fact that Langmuir waves drift to smaller wave-numbers, k, allowing them to increase their phase speed, $V_{ph}=\omega/k$, and, therefore, being subject to absorption by faster electrons.

This novel aspect electron acceleration has been explored in the plasma wake field acceleration context by Tsiklauri.[16] Thus, yet another motivation for the present work is to extend results of Tsiklauri[16] to tens of MeV range of electron energies and study the possibility of electron acceleration in the context of extreme solar flares.

In what follows, a brief overview of solar atmosphere physical parameters of relevance to this work is presented. The observational constraint on non-thermal electron densities in the chromosphere is the non-thermal hard X-ray (HXR) flux. However, this can be interpreted in at least two different ways:

(1) The chromospheric HXR flux can be expressed as a non-thermal emission measure, see, e.g., Brown *et al.*,[17] their Eqs. (2) and (3). Here, EM_{nt} tells us the *instantaneous* number density of non-thermal electrons in a

target of a given ambient number density. This is a model-independent interpretation (apart from the model for the bremsstrahlung cross section). Then, it is possible to find the ratio of the instantaneous number densities of non-thermal electrons (n_{nt}) to background density by comparing the non-thermal and thermal emission measures. Fletcher *et al.*[18] did this for one flare in and found that to explain the HXR observations $n_{nt}/n_{background} = 10^{-3}$–$10^{-4}$ should have $E > 15$ keV. But this ratio of course depends on where in the atmosphere the HXR emission is produced.

(2) One can interpret also the same chromospheric HXR flux measurement in a model-dependent way. In the collisional thick target model (without re-acceleration), the HXR flux measurement can be turned into a flux of electrons arriving at the top of the chromosphere of $\approx 10^{19-20}$ electrons $\mathrm{cm}^{-2}\,\mathrm{s}^{-1}$, e.g., Ref. 19. Dividing by the electron speed of $\approx 10^{10}$ cm s^{-1} gives a beam number density at the top of the chromosphere of 10^{9-10} electrons cm^{-3}. As the beam slows, n_{beam} (electron beam number density) remains constant so $n_{background}$ increases, until the beam thermalises. Thus, in this model-dependent interpretation the fraction number density can vary from $n_{beam}/n_{background} \geq 1$ at the top of the chromosphere to $n_{beam}/n_{background} \ll 1$ where the beam stops. One should bear in mind also that there is no strong evidence for anisotropic electron distributions (beams) in the chromosphere (e.g., Refs. 20 and 21).

Generally, the electron energies required to make the non-thermal HXR emission in the chromosphere via bremsstrahlung are of the order of tens of keV—speeds of 0.1–0.3c. This is far less extreme than the above mentioned tens of MeV flare observations. There are some results that show that HXR sources are apparently co-spatial with white-light sources and produce rather low in the atmosphere between 300 km and 800 km, cf.[22,23] The photospheric umbral fields can go up to 0.2–0.3 T, and flare sources are also seen in umbrae. The majority of flare emission, including HXR emission, is chromospheric, but there are no observations in which we can unambiguously say that the flare does not involve the corona in some way. We always see some coronal signature. However, is that evidence enough to say that the energy release location is coronal? The answer seems uncertain. Thus, there is a good reason to investigate electron re-acceleration low in the chromosphere. For example, the work on the low-altitude HXR and white light sources is a motivation, as currently there is no consensus how to get electrons accelerated in the corona down to that level, so the implication is that they could be accelerated locally. It should be noted that electron re-acceleration is of relevance not only to solar flares. Brunetti and Lazarian[24] calculate the acceleration of both protons and electrons taking into account both transit time damping acceleration and non-resonant acceleration by large-scale compressions. They find that relativistic electrons can be re-accelerated in the intracluster galactic medium (ICM) up to energies of several GeV.

Section II presents the model and results. Section III summarises the main findings.

II. THE MODEL AND RESULTS

The simulation is carried out using EPOCH, a fully electromagnetic (EM), relativistic PIC code.[25] EPOCH is available for download from https://cfsa-pmw.warwick.ac.uk. The mass ratio in all runs is $m_i/m_e = 1836.153$ and boundary conditions are periodic.

The simulations domain is split into $n_x \times n_y \times n_z = 1500 \times 72 \times 72$ grid cells in x-, y-, and z-directions, respectively. Each grid size is chosen to be Debye length (λ_D) times appropriate factor (f) long. Here, $\lambda_D = v_{th,e}/\omega_{pe}$ denotes the Debye length with $v_{th,e} = \sqrt{k_B T/m_e}$ being the electron thermal speed and ω_{pe} the electron plasma frequency. This means that as plasma temperature and density are varied so does the grid size. In the plasma wake field acceleration, the relevant spatial scale is electron inertial length c/ω_{pe}. We vary factor f such that: (i) in the solar coronal run, c/ω_{pe} is resolved with 12 grid points, i.e., $(c/\omega_{pe})/\Delta = 12.83$, where $\Delta = f \times \lambda_D$ is the grid size; (ii) in solar chromosphere run, c/ω_{pe} is resolved with also 12 grid points, i.e., $(c/\omega_{pe})/\Delta = 12.43$. This choice seems to provide a reasonable resolution since the energy error is small $\approx 0.017\% - 0.025\%$ for the both runs. Note that $f = 6$ in the coronal run and $f = 40$ in the chromospheric run.

The trailing and driving electron *bunches* have the number densities as follows:

$$n_T(x) = n_0 \times \exp\left[-\frac{\left(x - 10.0c/\omega_{pe}\right)^2}{2.0\left(2.0c/\omega_{pe}\right)^2}\right] \times \exp\left[-\frac{\left(y - y_{max}/2.0\right)^2}{2.0\left(c/\omega_{pe}\right)^2}\right] \times \exp\left[-\frac{\left(z - z_{max}/2.0\right)^2}{2.0\left(c/\omega_{pe}\right)^2}\right], \quad (1)$$

$$n_D(x) = 2.5n_0 \times \exp\left[-\frac{\left(x - 16c/\omega_{pe}\right)^2}{2.0\left(c/\omega_{pe}\right)^2}\right] \times \exp\left[-\frac{\left(y - y_{max}/2.0\right)^2}{2.0\left(c/\omega_{pe}\right)^2}\right] \times \exp\left[-\frac{\left(z - z_{max}/2.0\right)^2}{2.0\left(c/\omega_{pe}\right)^2}\right]. \quad (2)$$

These expressions imply that trailing bunch is centered on $10.0c/\omega_{pe}$ and has an x-length of $\sigma_x = 2.0c/\omega_{pe}$, while driving bunch is 2.5 denser than both the background and trailing bunch, is centered on $16.0c/\omega_{pe}$, and has an x-length of $\sigma_x = c/\omega_{pe}$. The distance between the trailing and driving bunches is $6.0c/\omega_{pe}$. Both electron bunches have y- and z-lengths of $\sigma_{y,z} = c/\omega_{pe}$ and are centered on $y = y_{max}/2$ and $z = z_{max}/2$.

Both electron bunch initial momenta are set to $p_x = p_0 = \gamma m_e 0.9999c\,\mathrm{kg\,m\,s}^{-1}$ (note that $p_x/(m_e c) = 70.70$, i.e., $\gamma = 70.70$), which corresponds to an initial energy of $E_0 = 36.12$ MeV. There are four plasma species (background

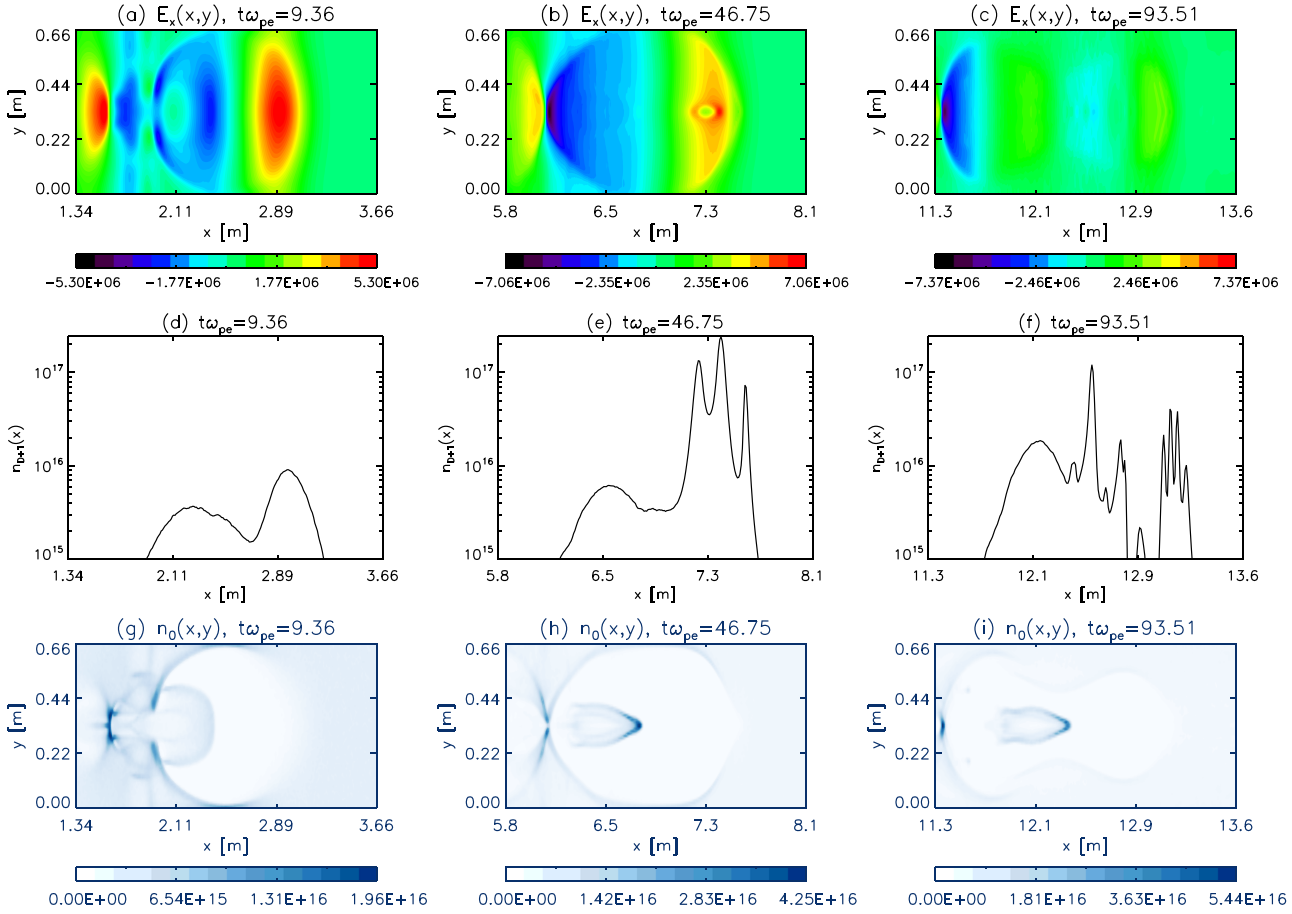

FIG. 1. (a)–(c) Contour plots of the electric field x-component in the (x,y) plane (cut through $z = z_{max}/2$) at different time instants corresponding to 1/10th, half, and the final simulation times. (d)–(f) log normal plot of the sum of driving and trailing electron bunch number densities at the same times. (g)–(i) Contour plots of background electron number density, in units of m^{-3}, in the (x,y) plane (cut through $z = z_{max}/2$) at the same times. The fields on color bars are quoted in V/m and time at the top of each panel is in ω_{pe}. The data are for solar coronal parameters. See text for details.

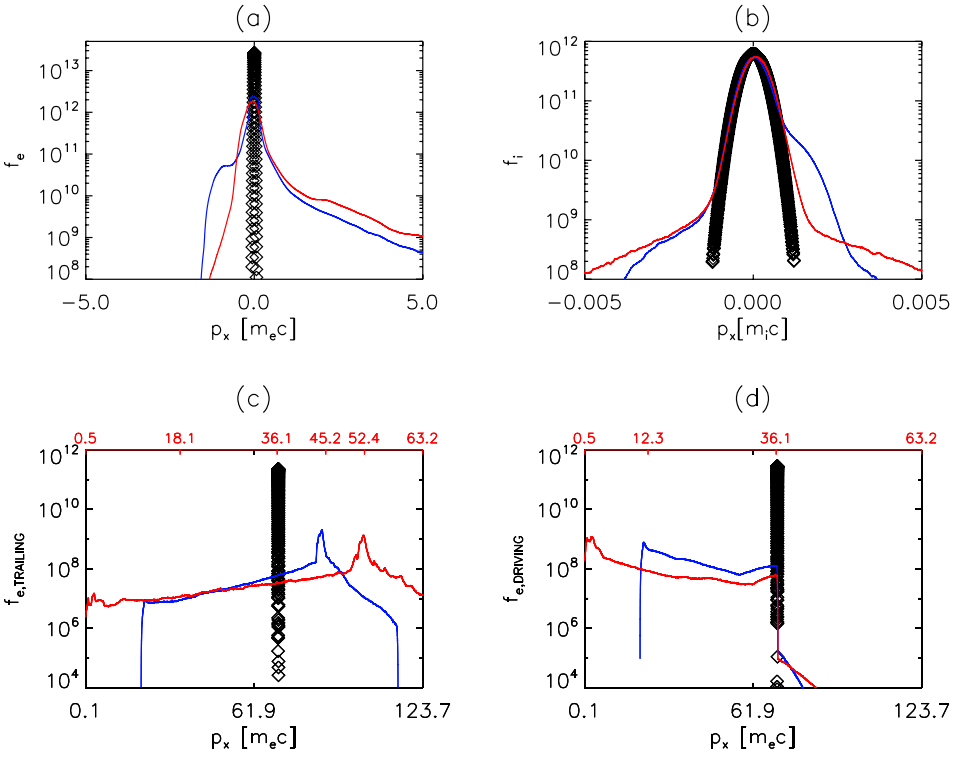

FIG. 2. Background electron (a), ion (b), trailing (c), and driving (d) electron bunch distribution functions at different times: open diamonds correspond to $t = 0$, while blue and red curves correspond to the half and the final simulations times, respectively. The x-axis is momenta quoted in the units of relevant species mass times speed of light, i.e., $[m_e c]$ or $[m_i c]$ as shown in each panel. In panels (c) and (d), at the top, the energy is quoted in MeV with red numbers, to aid eye visualization of trailing bunch acceleration and driving bunch deceleration processes. The data are for solar coronal parameters.

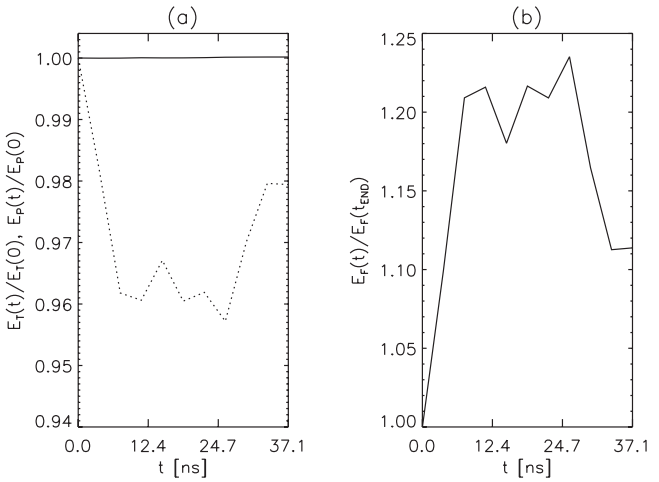

FIG. 3. In panel (a), solid and dashed curves are the total (particles plus EM fields) and particle energies, normalized on initial values, respectively. Panel (b) shows EM field energy, including background magnetic field of 0.01 T, normalized on its initial simulation time value. The data are for solar coronal parameters. The plot is produced with 10 data points, and time is nano-seconds (ns).

electrons and ions plus driving and trailing bunches) present in all numerical simulations. In the numerical runs, there are 279 936 000 particles for each of the four species, i.e., roughly 1.12×10^9 particles in total. The three dimensional runs take about 11 h on 288 computing cores, using AMD Interlagos 48-core CPUs with 64 Gb of random access memory and QDR Infiniband.

A. The case of solar coronal plasmas

In solar coronal parametric run, uniform density is set to $n_e = n_i = n_0 = 2 \times 10^{15}$ m^{-3} and temperature to $T = 10^6$ K. Both electron bunch temperatures are also set to $T_b = 10^6$ K. The uniform magnetic field along the x-axis is 0.01 T.

Figure 1 (top row) shows contour plots of electric field E_x component at three times. It can be seen that at $t\omega_{pe} = 9.36$ the yellow half-ellipse, representing positive $E_x \approx 5 \times 10^6$ V/m plasma, is followed by blue void of a complex shape with similar amplitude $E_x \approx -$few $\times 10^6$ V/m. Panels (a) to (c) show a moving window that has a length of $250\Delta = 250 f \lambda_D$ and a width of $72\Delta = 72 f \lambda_D$ that follows the driving and trailing bunches with a speed of $0.9999c$. Bulanov *et al.*[26] discuss two effects that impede efficient acceleration: (i) depletion of either driving laser pulse or electron bunch and (ii) de-phasing of the trailing electron bunch from the negative electrostatic E_x plasma wake. Obviously, it is only $E_x < 0$ that accelerates the electrons. On the contrary, $E_x > 0$ results in deceleration of the trailing electron bunch. Both the electron slippage with respect to the accelerating phase of the wake wave and the driving bunch/laser pulse energy depletion are important. The dephasing and depletion lengths are inversely proportional to the plasma density, and both are of the same order.[26] We gather that the both effects are clearly present in panels (a)–(f) of Fig. 1. In particular, we see in panels (a)–(c) that plasma wake strength fades away. However, we note that in

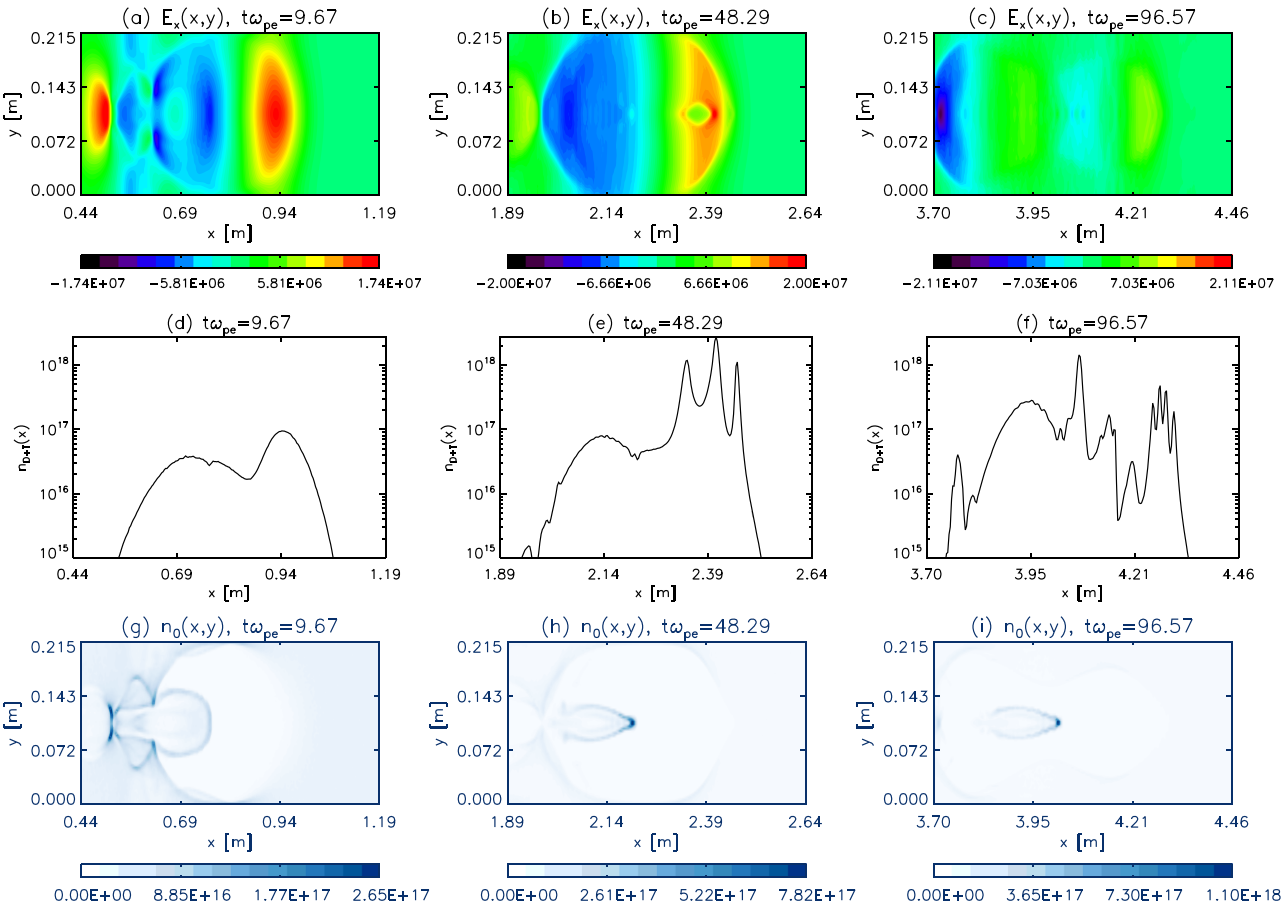

FIG. 4. As in Fig. 1 but for the case of solar chromospheric parameters. See text for details.

Fig. 1(c) rather compact negative wake near left edge gains strength to $E_x \approx -7.4 \times 10^6$ V/m. In panels (d)–(f), we see that initially [panel (d)] driving bunch, the right, taller bump, is co-spatial with positive (red-yellow) E_x and trailing bunch, the left, wide-and-short bump, is co-spatial with negative (blue) E_x. This implies that driving bunch will be decelerating, while trailing bunch will be accelerating, given the sign of E_x. By the end of simulation time $t\omega_{pe} = 93.51$ in panel (f), the trailing bunch has de-phased from the plasma wake considerably. From the panels (g)–(i), we gather that initially there was a substantial cavity created in the background electrons, but it depletes by the end of simulation.

In Fig. 2, the details of background electron, ion, trailing, and driving electron bunch distribution functions are quantified at different times: open diamonds correspond to $t = 0$, while blue and red curves to the half and the final simulations times, respectively. It can be gathered from the plot [panel (a)] that the background electrons develop non-thermal tails in the direction of motion of the trailing and driving electron bunches (i.e., positive x-direction) with values attaining $p_x \approx 5\ m_e c$. Ions [panel (b)] initially show beaming in the positive p_x direction (blue curve), but by the end of simulation (red curve), ions develop non-thermal tails. Note that the bulk of the distribution does not show significant broadening, only nonthermal tails. Panel (c) demonstrates that by the end of simulation time, the trailing bunch gains energy to 52 MeV (red curve), starting from initial 36.1 MeV. Recall that $\gamma = 70.70$ corresponds to the initial energy of $E_0 = 36.12$ MeV. Panel (d) demonstrates that by the end of simulation time, the driving bunch loses energy to 0.5 MeV (red curve), starting from initial 36.1 MeV. This serves as a proof that trailing electron bunch acceleration is on the expense of driving bunch deceleration. The same conclusion can be drawn from the behaviour of different kinds of energies in the next plot.

Panel (a) of Fig. 3 shows the behavior of the total (particles plus EM fields) and particle energies, normalized to initial values, respectively. The total energy increases due to numerical heating, but remains within a tolerable value of 0.017%, i.e., $E_T(t)/E_T(0)$ starts from unity and increases to 1.00017. The particle energy decreases by 4% by mid-simulation time and then bounces back to 0.98 of the initial value. This points to the fact that the process is intermittent in time. The reason for such time-transient behaviour is in both (i) depletion of electron bunch and (ii) de-phasing of the trailing electron bunch from the negative electrostatic E_x plasma wake. Panel (b) shows EM field energy normalized to its initial simulation time value. It can be seen that it experiences time-transient increases as the plasma wake is generated and then depleted.

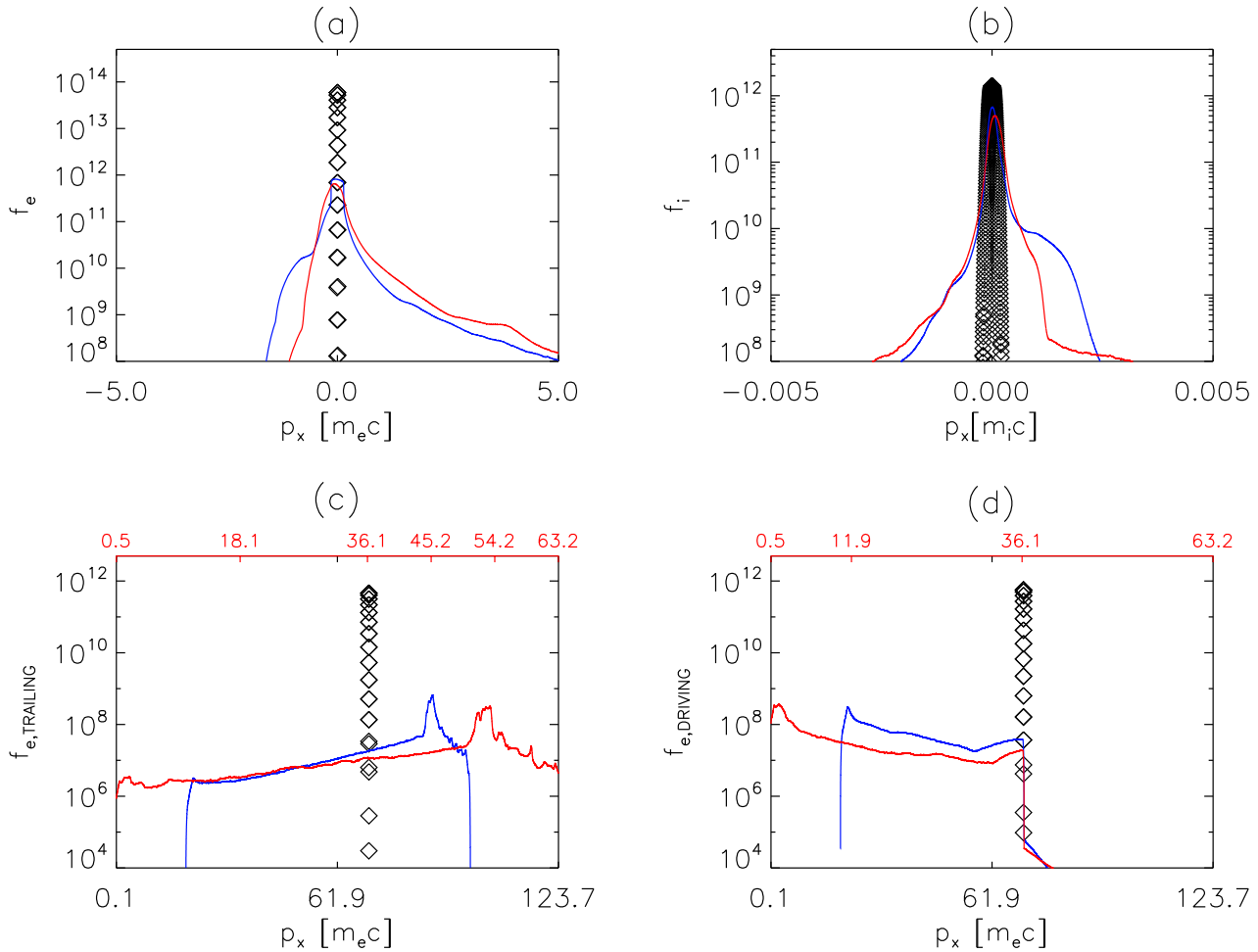

FIG. 5. As in Fig. 2 but for the case of solar chromospheric parameters.

B. The case of solar chromospheric plasmas

In the solar chromosphere parametric run, uniform density is set to $n_e = n_i = n_0 = 2 \times 10^{16}\,\mathrm{m}^{-3}$ and temperature to $T = 2.4 \times 10^4$ K. This corresponds to the top of the chromosphere and similar values were used by Tsiklauri and Pechhacker,[27] in a different context. Both electron bunch temperatures are also set to $T_b = 2.4 \times 10^4$ K. The uniform magnetic field along the x-axis is 0.02 T.

Figure 4 is similar to Fig. 1 but for the case of solar chromosphere parameters. It can be gathered from panels (a)–(c) of Fig. 4 that electrostatic plasma wake becomes spatially localized (note the different spatial extent on x- and y-axes) and, compared to the coronal case, E_x now attains $\sqrt{10}$ larger values of $\pm 1.74 \times 10^7$ V/m. This can be explained by the fact that the plasma wake size is prescribed by the electron inertial length, c/ω_{pe}. Hence, because of the scaling law $\omega_{pe} \propto \sqrt{n_e}$, larger density, into which driving bunch plows through, creates more localized and stronger plasma wake. Panels (d)–(f) show similar bunch de-phasing as in Fig. 1, but now density peak in panel (e) is 10 times higher, as the density in the chromosphere was chosen to be also 10 times larger. Panels (g)–(i) also show initial creation and subsequent draining of the background electron density cavity, except with 20 times larger localised density [note maximum scale in Fig. 4(i)].

Figure 5 is similar to Fig. 2 but for the case of solar chromosphere parameters. We note in panels (a)–(b) of Fig. 5 that background electrons and ions have similar response to the injection of the driving electron bunch, except that superthermal tails are less prominent. Note also that ion peak at $t = 0$, represented by open diamonds in panel (b) of Fig. 5, is narrower than in Fig. 2, as the background plasma temperature is significantly cooler ($T = 2.4 \times 10^4$ K). The weaker chromospheric background plasma response can be understood by its higher density and cooler temperature. The trailing bunch acceleration and driving bunch deceleration in the chromospheric case bear the close similarities to the coronal one [as panels (c)–(d) of Fig. 5 are similar to Fig. 2]. We should bear in mind that the actual domain and thus acceleration length are quite different in both cases: in the solar corona $x_{\max} = 1500\Delta = 1500 f \lambda_D = 13.888$ m, while in the chromosphere $x_{\max} = 1500\Delta = 1500 f \lambda_D = 4.536$ m. The end simulation time in both runs is fixed at $0.8 \times 1500 f \lambda_D / c$, so that the trailing and driving bunches never reach simulation domain boundaries, while traversing its 0.8 length.

Figure 6 is similar to Fig. 3 but for the case of chromospheric run. Here, the total energy error is 0.025% (i.e., $E_T(t)/E_T(0)$ starts from unity and increases to 1.00025). This is larger than in the coronal run case but still tolerable. The behaviour of various kinds of energies is similar to that in Fig. 3 in that there is still a time transient decrease in the particle and increase in the EM energy. The notable difference now is that solid curve in the right panel peaks at 1.5. In the coronal case (Fig. 3), it peaked at 1.2. Note also that background magnetic fields (used in the normalization) in the both cases are also different. The stronger peak can be understood by a stronger/denser wake generated in more dense chromospheric plasmas.

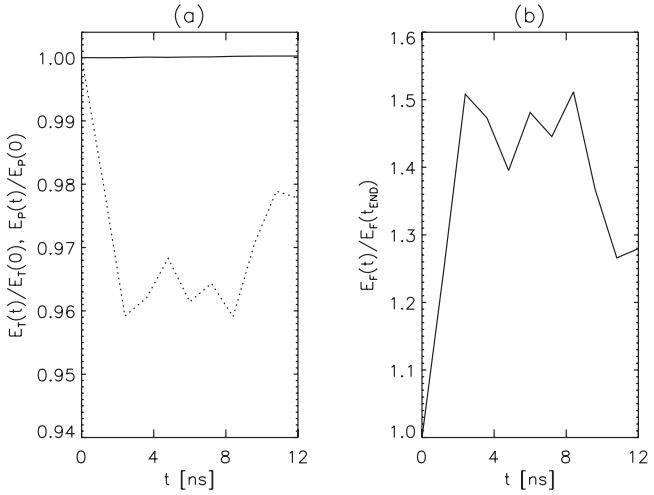

FIG. 6. As in Fig. 3 but for the case of solar chromospheric parameters. Here, $B_0 = 0.02$ T.

III. CONCLUSIONS

This work presents 3D, particle-in-cell, fully electromagnetic simulations of electron plasma wake field acceleration applicable to the solar atmosphere. It was shown that injecting driving and trailing electron bunches into solar coronal and chromospheric plasmas results in electric fields ($-(20-5) \times 10^6$ V/m). This leads to acceleration of the trailing bunch up to 52 MeV, starting from initial 36 MeV. It is suggested that the present results provide one of the potentially important mechanisms for the extremely energetic solar flare electron acceleration by means of the plasma wake field acceleration. It should be noted, however, that there may exist alternative scenarios. For example, it is well known that the magnetic reconnection of solar coronal fields (see e.g., Tajima and Shibata[28]) can give rise to strong field-aligned electric fields. Such fields could also give rise to a mechanism of accelerating electrons to high energies. Similar examples may be found in the geomagnetic field implication of reconnection (e.g., Wagner *et al.*[29]). Other examples may be found in the direct current (DC) field acceleration due to reconnection fields including laboratory plasmas (e.g., Leboeuf *et al.*[30,31]).

ACKNOWLEDGMENTS

This research utilized Queen Mary University of London's (QMUL) MidPlus computational facilities, supported by QMUL Research-IT and funded by UK EPSRC Grant No. EP/K000128/1.

[1]D. B. Melrose and J. C. Brown, Mon. Not. R. Astron. Soc. **176**, 15 (1976).
[2]J. Steinacker, R. Schlickeiser, and W. Droge, Sol. Phys. **115**, 313 (1988).
[3]M. J. Aschwanden, *Physics of the Solar Corona: An Introduction with Problems and Solutions*, 2nd ed. (Praxis, Chichester, UK, 2005).
[4]W. T. Vestrand, G. H. Share, R. J. Murphy, D. J. Forrest, E. Rieger, E. L. Chupp, and G. Kanbach, Astrophys. J. Suppl. Ser. **120**, 409 (1999).
[5]D. Moses, W. Droege, P. Meyer, and P. Evenson, Astrophys. J. **346**, 523 (1989).
[6]T. Tajima and J. M. Dawson, Phys. Rev. Lett. **43**, 267 (1979).
[7]C. Joshi, W. B. Mori, T. Katsouleas, J. M. Dawson, J. M. Kindel, and D. W. Forslund, Nature **311**, 525 (1984).

[8]M. Litos, E. Adli, W. An, C. I. Clarke, C. E. Clayton, S. Corde, J. P. Delahaye, R. J. England, A. S. Fisher, J. Frederico *et al.*, Nature **515**, 92 (2014).
[9]M. J. Hogan, T. O. Raubenheimer, A. Seryi, P. Muggli, T. Katsouleas, C. Huang, W. Lu, W. An, K. A. Marsh, W. B. Mori *et al.*, New J. Phys. **12**, 055030 (2010).
[10]T. Ebisuzaki and T. Tajima, Astropart. Phys. **56**, 9 (2014), ISSN 0927-6505.
[11]T. Ebisuzaki and T. Tajima, Eur. Phys. J.: Spec. Top. **223**, 1113 (2014), ISSN 1951-6401.
[12]C. K. Lau, P. C. Yeh, O. Luk, J. McClenaghan, T. Ebisuzaki, and T. Tajima, Phys. Rev. ST Accel. Beams **18**, 024401 (2015).
[13]D. M. Farinella, C. K. Lau, X. M. Zhang, J. K. Koga, S. Taimourzadeh, Y. Hwang, K. Abazajian, N. Canac, T. Ebisuzaki, P. Taborek *et al.*, Phys. Plasmas **23**, 073107 (2016).
[14]T. Tajima, K. Nakajima, and G. Mourou, Rev. Nuevo Cimento **40**, 33 (2017).
[15]R. Pechhacker and D. Tsiklauri, Phys. Plasmas **21**, 012903 (2014).
[16]D. Tsiklauri, Proc. R. Soc. London, Ser. A **472**, 20160630 (2016).
[17]J. C. Brown, R. Turkmani, E. P. Kontar, A. L. MacKinnon, and L. Vlahos, Astron. Astrophys. **508**, 993 (2009).
[18]L. Fletcher, I. G. Hannah, H. S. Hudson, and D. E. Innes, Astrophys. J. **771**, 104 (2013).
[19]S. Krucker, H. S. Hudson, N. L. S. Jeffrey, M. Battaglia, E. P. Kontar, A. O. Benz, A. Csillaghy, and R. P. Lin, Astrophys. J. **739**, 96 (2011).
[20]E. P. Kontar and J. C. Brown, Astrophys. J. Lett. **653**, L149 (2006).
[21]J. Kasparova, E. P. Kontar, and J. C. Brown, Astron. Astrophys. **466**, 705 (2007).
[22]J.-C. Martinez Oliveros, H. S. Hudson, G. J. Hurford, S. Krucker, R. P. Lin, C. Lindsey, S. Couvidat, J. Schou, and W. T. Thompson, Astrophys. J. Lett. **753**, L26 (2012).
[23]S. Krucker, P. Saint-Hilaire, H. S. Hudson, M. Haberreiter, J. C. Martinez-Oliveros, M. D. Fivian, G. Hurford, L. Kleint, M. Battaglia, M. Kuhar *et al.*, Astrophys. J. **802**, 19 (2015).
[24]G. Brunetti and A. Lazarian, Mon. Not. R. Astron. Soc. **378**, 245 (2007).
[25]T. D. Arber, K. Bennett, C. S. Brady, A. Lawrence-Douglas, M. G. Ramsay, N. J. Sircombe, P. Gillies, R. G. Evans, H. Schmitz, A. R. Bell *et al.*, Plasma Phys. Controlled Fusion **57**, 113001 (2015).
[26]S. V. Bulanov, T. Z. Esirkepov, Y. Hayashi, H. Kiriyama, J. K. Koga, H. Kotaki, M. Mori, and M. Kando, J. Plasma Phys. **82**, 905820308 (2016).
[27]D. Tsiklauri and R. Pechhacker, Phys. Plasmas **18**, 042901 (2011).
[28]T. Tajima and K. Shibata, *Plasma Astrophysics* (Perseus, Cambridge, Mass, 2002).
[29]J. S. Wagner, J. R. Kan, S.-I. Akasofu, T. Tajima, J. N. Leboeuf, and J. M. Dawson, Phys. Rev. Lett. **45**, 803 (1980).
[30]J. N. Leboeuf, T. Tajima, and J. M. Dawson, Phys. Rev. Lett. **43**, 1321 (1979).
[31]J. N. Leboeuf, J. M. Dawson, S. T. Ratliff, M. Rhodes, and N. C. Luhmann, Jr., Phys. Fluids **25**, 2045 (1982).